crystals

MDPI

Letter

Formation of GaAs/GaSb Core-Shell Heterostructured Nanowires Grown by Molecular-Beam Epitaxy

Dong-Dong Wei [1,2], Sui-Xing Shi [2], Chen Zhou [3], Xu-Tao Zhang [2], Ping-Ping Chen [2,*], Jing-Tao Xie [4], Feng Tian [1] and Jin Zou [3,5]

1 School of Materials Science and Engineering, University of Shanghai for Science and Technology, 516 Jun-Gong Road, Shanghai 200093, China
2 National Laboratory of Infrared Physics, Shanghai Institute of Technical Physics, Chinese Academy of Science, 500 Yu-Tian Road, Shanghai 200083, China
3 School of Engineering, The University of Queensland, St. Lucia, QLD 4072, Australia
4 Laboratory of Advanced Materials, Fudan University, Shanghai 200438, China
5 Center for Microscopy and Microanalysis, The University of Queensland, St. Lucia, QLD 4072, Australia
* Correspondence: ppchen@mail.sitp.ac.cn

Academic Editor: Paul J. Simmonds
Received: 28 February 2017; Accepted: 22 March 2017; Published: 24 March 2017

Abstract: In this paper, we demonstrated the growth of GaAs/GaSb core-shell heterostructured nanowires on GaAs substrates, with the assistance of Au catalysts by molecular-beam epitaxy. Time-evolution experiments were designed to study the formation of GaSb shells with different growth times. It was found that, by comparing the morphology of nanowires for various growth times, lateral growth was taking a dominant position since GaSb growth began and bulgy GaSb particles formed on the nanowire tips during the growth. The movement of catalyst Au droplets was witnessed, thus, the radial growth was enhanced by sidewall nucleation under the vapor-solid mechanism due to the lack of driving force for axial growth. Moreover, compositional and structural characteristics of the GaAs/GaSb core-shell heterostructured nanowires were investigated by electron microscopy. Differing from the commonly anticipated result, GaSb shells took a wurzite structure instead of a zinc-blende structure to form the GaAs/GaSb wurzite/wurzite core-shell heterostructured nanowires, which is of interest to the research of band-gap engineering. This study provides a significant insight into the formation of core-shell heterostructured nanowires.

Keywords: GaSb; core-shell heterostructure; diffusion behavior; semiconductor III-V materials; molecular-beam epitaxy (MBE)

1. Introduction

III-V semiconductor nanowires (NWs) have been studied extensively in recent years due to their unique physical properties [1,2] and, in turn, have been used in a wide range of applications, including solar cells [3–5], nanolasers [6], infrared detectors [7–9], and quantum computing [10,11]. With their growth feature of being free-standing, NWs can withstand much higher lattice mismatch, since the strain at the hetero-interface between two different materials can be elastically relieved easily [12]. Moreover, owing to the large surface-to-volume ratio, NWs have superior performance in biosensors [13] and photoelectrochemical energy conversion [14]. Thus, NWs can be an effective solution to the preparation of semiconductor heterostructures for device applications.

To date, many growth mechanisms have been proposed to explain and synthesize these semiconductor NWs, including vapor-liquid-solid (VLS), vapor-solid (VS), oxide-assisted, and solution-liquid-solid [15]. VLS mechanism has been the most widely used mechanism for NW growth because it helps to synthesize axial [16,17] and branched heterostructure NWs [18] with

control over their size, shape, and location, while VS mechanism was proposed to explain NW lateral growth [19,20]. Radial heterostructure NWs, consisting of core, shell or multiple shell layers, provide a new path to tailor the band-gap structure, which is essential for band-gap engineering.

In particular, III-V NWs with core-shell heterostructure possess some attractive characteristics which are promising as applications to the NW-based optical and electrical devices in the future. The NW shells would passivate the NW inner core by suppressing the surface state. Since the surface state would degrade the performance of III-V NW-based devices on electrical transportation and light emission through scattering and a nonradiative recombination process [21,22]. Similar were results were reported on GaAs/AlGaAs [23–25], GaAs/GaInP [26], and InAs/InP [21] NWs with core-shell heterostructures. Besides, the type II and III band alignment of GaAs/GaSb and InAs/GaSb can help to produce the accumulation of the carriers on the core-shell interface of the heterostructures, achieving a high concentration of the carriers without the intended doping [27]. Furthermore, the transportation path and the charge carrier type of GaSb/InAsSb core-shell NWs can be tuned by changing the thickness of the NW shells and the applied bias voltage [28]. According to recent reports about InAs/InSb [29] and GaAs/GaSb [30], research has been mainly focused on axial heterostructures, while there are few reports about core-shell NWs.

In this study, we designed a set of time-evolution experiments to understand the formation of GaAs/GaSb core-shell heterostructured NWs grown by molecular-beam epitaxy (MBE) via the assistance of Au catalyst. Four NW samples were grown by controlling the deposition time of GaSb. The structural and compositional characteristics of the grown NWs were studied by detailed electron microscopy. It is found that both GaAs cores and GaSb shells possess the wurzite crystal structure. Moreover, bulgy GaSb particles formed on the NW tips while the Au alloy catalyst diffused away when the growth of the GaSb section commences. The growth mechanism of this wurzite structure of the GaAs/GaSb core-shell NWs is discussed.

2. Results and Discussion

Figure 1 shows scanning electron microscopy (SEM) images taken from four samples with different deposition times of GaSb, among which images of pure GaAs NWs were taken for comparison to understand the growth of GaSb shells. As can be seen from Figure 1a, vertical GaAs NWs with a high density are observed with consistent morphology and orientation. They are 700–800 nm in length, with diameters ranging from 30–50 nm. Additionally, slight tapering can be clearly witnessed, especially in the bottom region, suggesting that lateral growth occurred [31,32]. Figure 1b is a side view SEM image of grown GaAs/GaSb NWs with a 1 min growth time of GaSb. The insert is a magnified SEM image of typical NWs, showing rugged sidewalls and evident particles on NW tips, compared with GaAs NWs in Figure 1a.

In Figure 1b, most of the NWs grow perpendicular to the substrate. A few inclined NWs were also found, probably because the existence of the catalyst supersaturation threshold, as different orientated NWs can be induced by tuning the III-Au concentration. A similar catalyst composition-induced growth has been discussed by Zhang et al. [33]. In Figure 1c,d, with the extension of the GaSb deposition time (5 min and 15 min), NW shells are proportionally increased, leading to wider diameters, which is indicative of the NWs' predominantly lateral growth. In the meantime, unlike traditional hemisphere-shaped catalyst droplets, bulgy particles are clearly noted on NW tips. It is of interest to note that, in Figure 1c, there are obvious bends in most NWs, while these short NWs still grow perpendicularly to the substrate. This is probably caused by asymmetry strain accumulation during the NW growth. Detailed growth mechanism will be discussed.

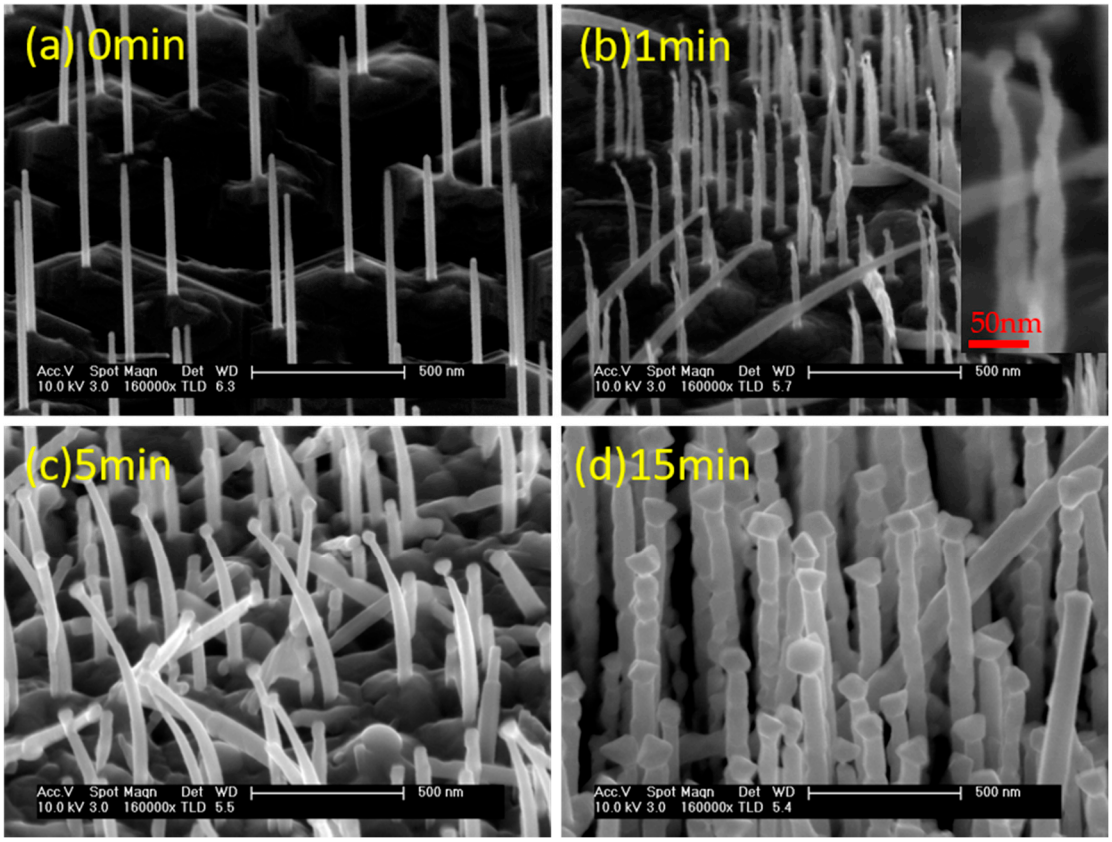

Figure 1. 45° Tilt SEM investigations of GaAs/GaSb heterostructure nanowires (NWs) with different growth times for the GaSb section: (**a**) 0 min, (**b**) 1 min, (**c**) 5 min, and (**d**) 15 min. Insert in (**b**) is a high magnification image of NWs. Scale bars are 500 nm in (**a**–**d**) and 50 nm in the insert of (**b**).

To understand detailed structural characteristics of the grown NWs, TEM investigations were performed. Figure 2a shows a bright-field transmission electron microscopy (TEM) image of a typical GaAs NW. Figure 2b,c are magnified TEM images taken from top of the NW, corresponding to the red regions in Figure 2a respectively, where the slight tapering caused by lateral growth is consistent with the SEM image shown in Figure 1a. Some planar defects can be seen in these magnified TEM images. Figure 2d is the high-resolution TEM image of the NW and the insert is the Fast Fourier Transform (FFT) result, from which the grown GaAs NWs possess wurzite structure. To understand the composition of the catalyst, energy dispersive spectroscopy (EDS) analysis was carried out and the result is shown in Figure 2e, in which the catalyst contains Au and Ga. Further quantitative EDS analysis shows that the Ga concentration in the catalyst is 7.4 at. %. Our extensive TEM observations match perfectly with previous reports that NW structure can be tuned by catalyst composition. Zhang et al. claimed that defect-free wurzite structure GaAs NWs can be acquired with a high Ga supersaturation in catalysts (~10%), while massive intermixing defects appear when the Ga concentration is only about 1% [34]. This explains our GaAs NW with few planar defects.

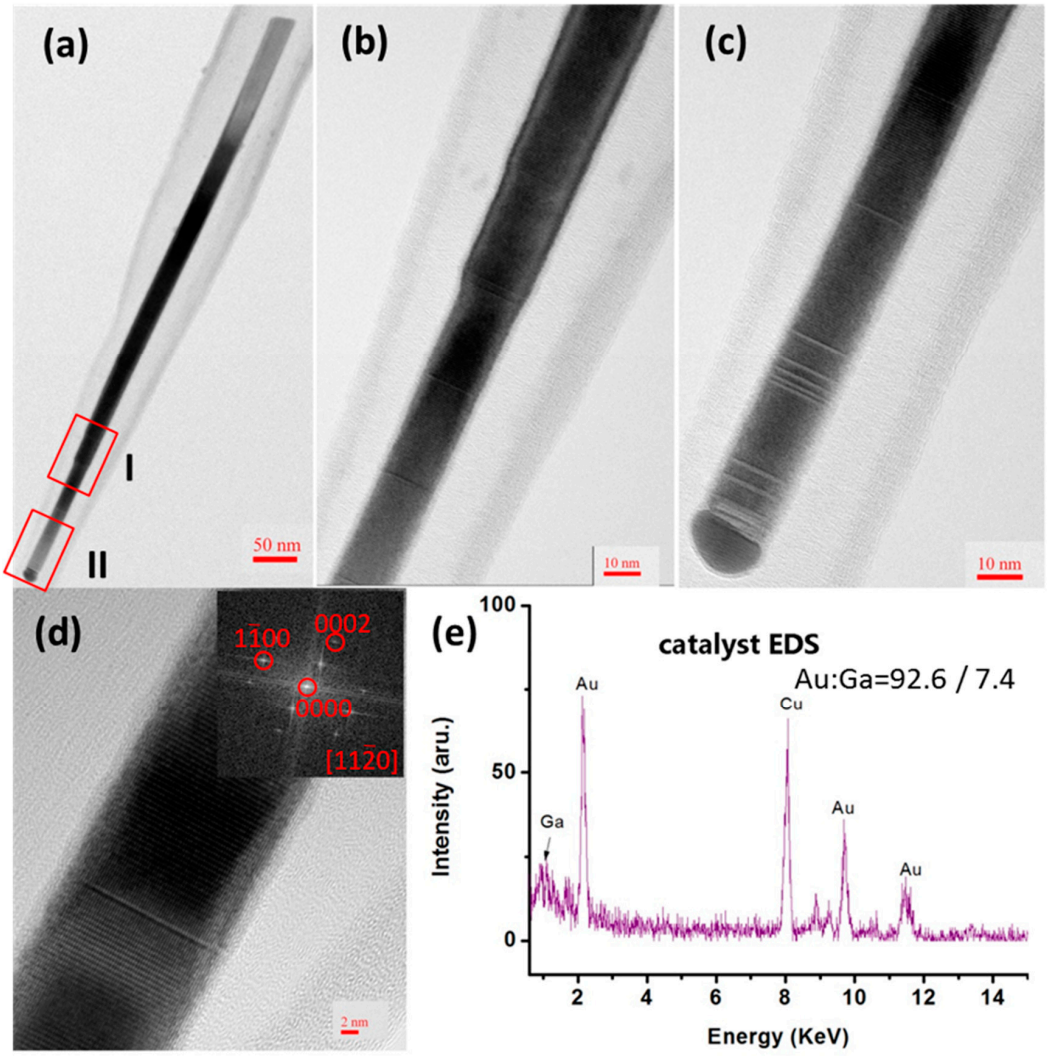

Figure 2. TEM characterizations of GaAs NWs. (**a**) Bright-field TEM image of typical GaAs NWs. (**b**,**c**) are high magnification images corresponding to the red region I and II respectively in (**a**). (**d**) High-resolution TEM image of the NW and the insert is the corresponding FFT result. (**e**) EDS spectra taken from the catalyst. Scale bars are 50 nm in (**a**), 10 nm in (**b**,**c**) and 2 nm in (**d**).

Figure 3 shows the TEM study of a typical GaAs/GaSb heterostructured NW, of which the growth time is 1 min for the GaSb section. The Moiré fringes on both sides are seen obviously throughout the entire NW, suggesting the formation of the core-shell structure. GaAs and GaSb have different lattice parameters, resulting in the strain contrast [35]. According to the high-resolution TEM image in Figure 3f, taken from the NW middle region indicated by the red line in Figure 3a, and the corresponding FFT in Figure 3g, the crystal structure of the NW can be determined to be a wurzite structure. The bulgy particle on top of the NW can be clearly observed in Figure 3e. To understand the composition of the bulgy particle on top and its underlying NW, EDS analysis was employed and the results are shown in Figure 3h, in which the particle is made of Ga and Sb, and below the particle is the GaAs NW. During the conventional growth of NWs, NWs are usually grown via the VLS mechanism on the surface activated by droplets of a catalyst, such as Au, Ag [36], and Al [37]. The droplet can act as catalyst for the precursor decomposition or it can strongly reduce the nucleation barrier. After growth, the droplet can still be obviously noted, as shown in Figure 2c. Meanwhile, different from conventional growth, we found that the particle on the NW top is GaSb rather than the Au alloy catalyst, meaning that the Au droplet has moved away from the NW top. The Au droplets obviously

remain on the NW tops during the GaAs growth, thus, this movement of Au droplets should happen during the GaSb growth.

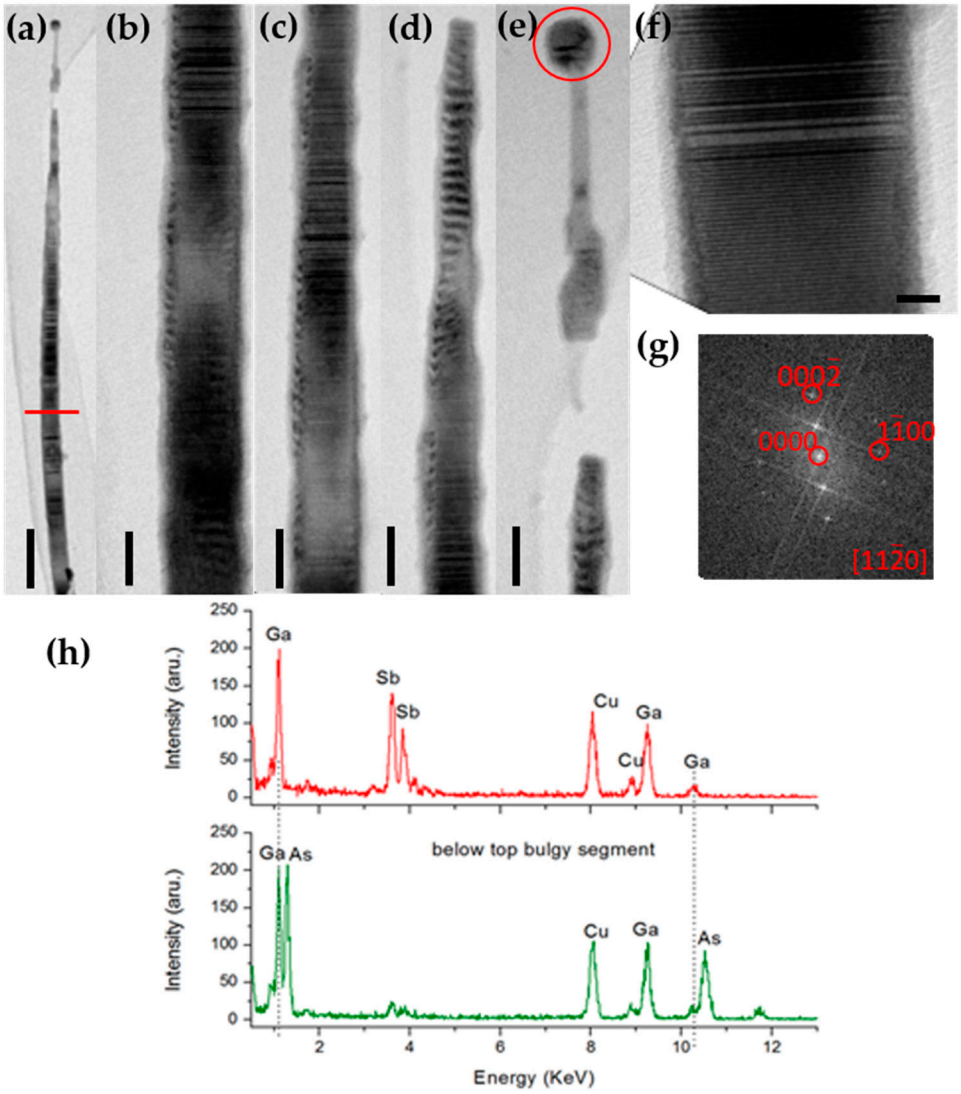

Figure 3. Detailed TEM investigation of a typical GaAs/GaSb NW with 1 min growth time. (**a**) Bright-field TEM image of the GaAs/GaSb NW. (**b**–**e**) High magnification image corresponding to different parts of the NW in (**a**) from bottom to top. (**f**) Corresponding high-resolution TEM image taken from the middle region of the NW, indicated by the red line in (**a**). (**g**) FET analysis taken from the region in (**f**). (**h**) EDS spectra taken from the catalyst and its underlying NW. Scale bars are 100 nm in (**a**), 20 nm in (**b**–**e**), and 5 nm in (**f**).

For further investigation, detailed TEM and EDS analyses were performed on NWs grown with 5 min growth time of GaSb. Figure 4a is a bright-field TEM image of a typical GaAs/GaSb NW. Figure 4b–d are magnified TEM images taken from different sections of the NW, corresponding to region I, II and III, respectively. The Moiré fringes appear throughout the NW and are even more obvious than those of the NW shown in Figure 3. Moreover, as can be seen in Figure 4a, together with previous SEM image of Figure 1c, the NWs show distinct curvature. From Figure 4b–d, asymmetric strain contrasts are noted by comparing both sides of the NW: a thin strip of strain contrast can be witnessed on the left side, while on the right side of the NW, apart from the Moiré fringes, some thicker

rugged and discontinuous shells can be found with much less obvious strain contrast, as indicated by arrows.

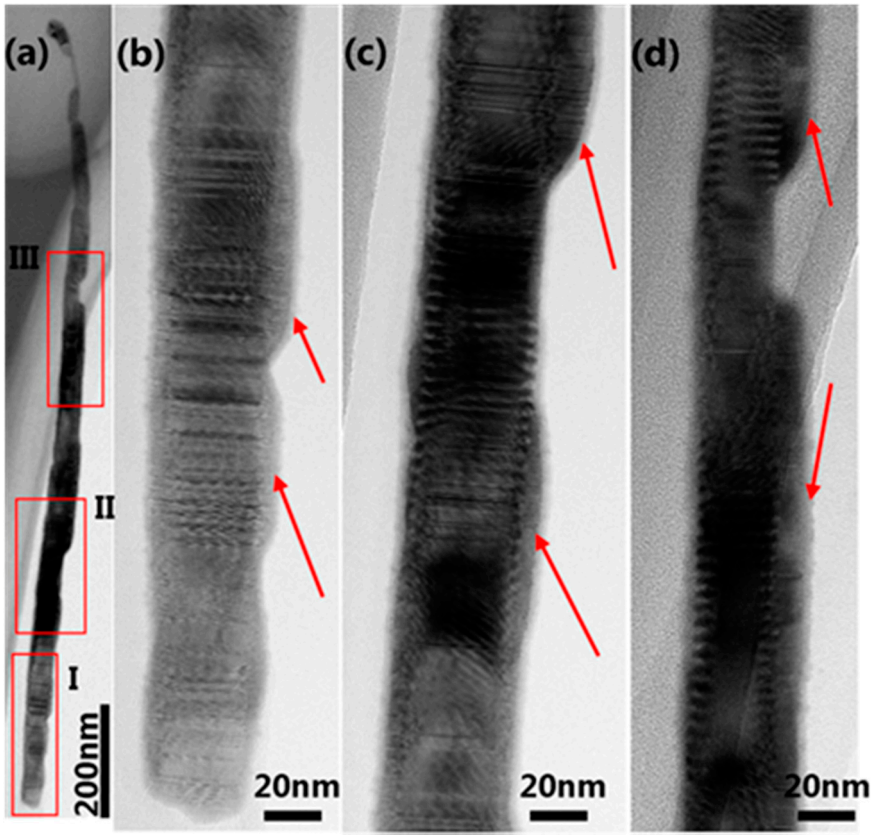

Figure 4. TEM characterizations of the GaAs/GaSb NW. (**a**) A bright-field TEM image of a typical GaAs/GaSb NW with 5 min growth time. (**b**–**d**) are high magnification images corresponding to I, II, III, as shown in (**a**), respectively. Scale bars are 200 nm in (**a**), 20 nm in (**b**–**d**).

Since the lattice parameter of GaSb (a = 6.0959 Å) is larger than that of GaAs (a = 5.6533 Å), more tensile stress will be produced on the thicker side of the shell when GaSb sheathes on the surface of GaAs, forcing the NW become concave toward thinner side of the shell. When NWs grow with little curvature, more growth species would be deposited on the convex surface, compared with the concave side, leading to more serious curvature. This can be also verified by the EDS data in Figure 5, especially in Figure 5c,d, corresponding to positions III and II of the NW in Figure 5a, respectively, where a much thicker shell can be observed. As the EDS scanned from left to right, two Sb peaks can be easily recognized and the left peak is stronger than the right one, meaning that a higher Sb concentration is on the left side than on the right side, i.e., a thicker GaSb shell formed on the left.

Thus, lattice mismatch between the core and shell increases together with the thickness of shell layer until relaxation, as long as the growth of GaSb continues, leading to strong asymmetry strain accumulation in the shell. Furthermore, discontinuous GaSb shell layers around GaAs cores are also noted both in Figures 3 and 4, which may be attributed to the variation of surface energetics, as well as surface contamination and native oxide [38].

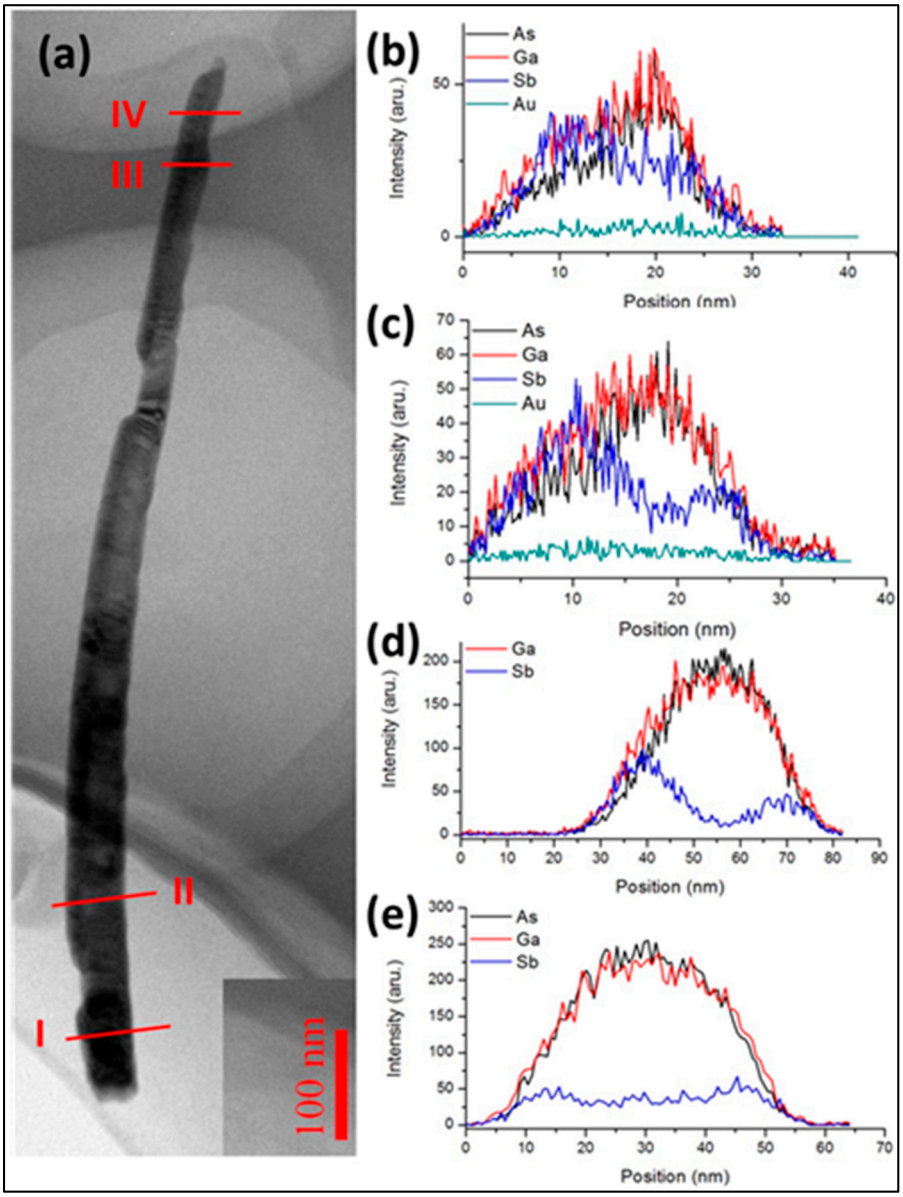

Figure 5. (**a**) A bright-field TEM image of GaAs/GaSb NW with 5 min growth time. (**b**–**e**) EDS line scan results corresponding to the GaAs/GaSb NW from top to bottom respectively, as indicated by the red line. Scale bar is 100 nm in (**a**).

As for former samples, the shell layers' crystal structure cannot be easily determined because of their short growth time. Thus, detailed TEM characterization was carried out on NWs with 15 min growth time of the GaSb section. Figure 6 is a high-resolution TEM image taken from a section of the core-shell region, in which a high density of lattice defects can be observed because of a large lattice mismatch (up to 7.5%) between GaAs and GaSb. According to the TEM image and the insert selective area electron diffraction (SAED) pattern taken from the shell region, the shell region can be determined to be a wurzite-dominant structure.

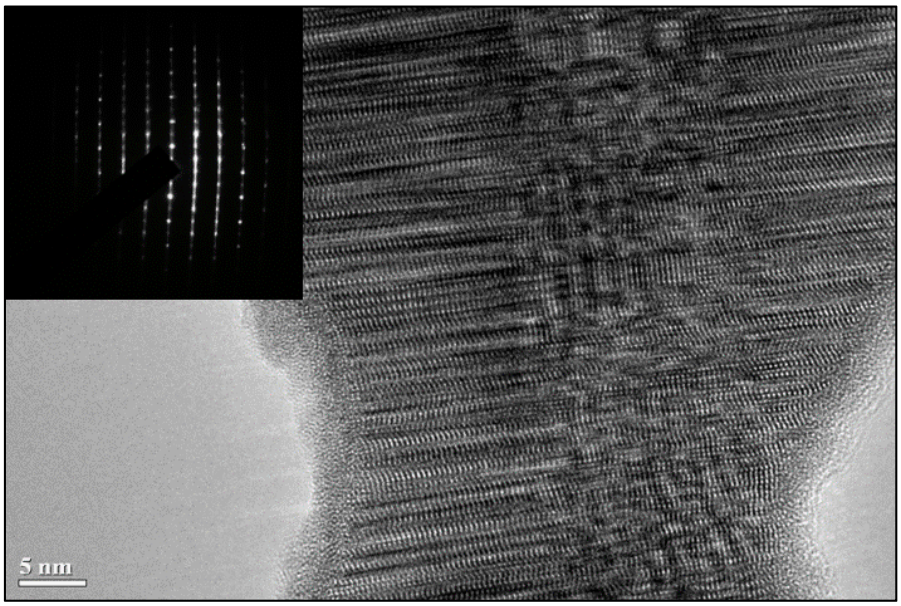

Figure 6. HRTEM demonstration of GaAs/GaSb NWs with SAED insert, of which the GaSb growth time is 15 min, and the scale bar is 5 nm.

In addition, since we have confirmed the formation of GaSb particles on NW tips, the locations of the Au catalyst droplets should be determined. As it can be seen from Figure 5b,c, the Au can barely be detected. Although detailed EDS analysis was performed on over a dozen of the core-shell NWs, in some cases a small particle was found in the side walls of the GaAs/GaSb NWs. Figure 7 shows an example. In Figure 7a, the particle marked by P1 shows distinct image contrast against other areas close-by, marked by P2 and P3, which were taken from sidewall and middle region, respectively, and placed close to the P1 position for better comparison. The particle was verified by EDS in Figure 7b, and this evidently illustrated that Au particles move downward during the GaSb growth. We account for this movement of Au particles in terms of growth kinetics, since the interfacial energy of Au-GaAs is different with Au-GaSb, which could interrupt the equilibrium of crystallization when Sb atoms entered into the Au particle, leading to the different morphology [16].

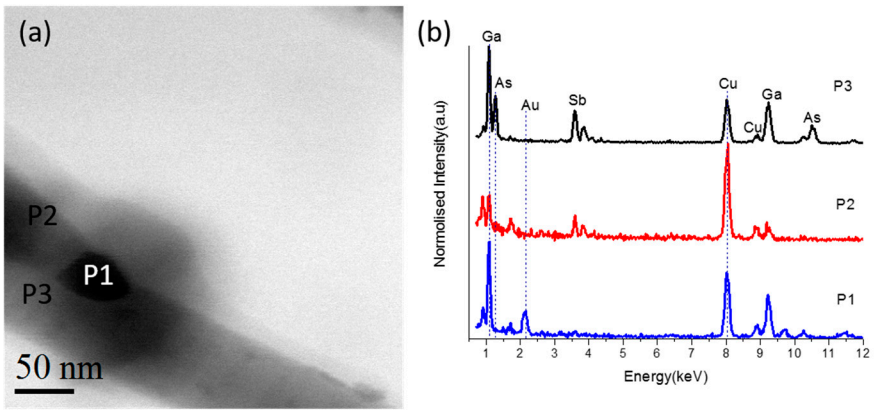

Figure 7. (**a**) TEM image taken from one segment of the GaAs/GaSb NW, in which the P1 position represents an Au particle. (**b**) Corresponding EDS line scans for the indicated P1, P2 and P3 in (**a**), respectively.

It has been well documented that the axial growth mode under VLS mechanism [3,4], as well as the lateral growth mode which is regulated by VS mechanism [19,20], are two dominating and

competing growth modes during the general Au-assisted growth of III-V NWs. For the axial growth of NWs by MBE, growth species are provided by surface adatoms diffusing towards the catalyst [39], and the chemical potential difference between the catalyst and the NW acts as the driving force. Nevertheless, GaSb cannot grow axially for the lack of Au catalyst particles, which makes it preferential for VS-dominated growth. Furthermore, it is liable for the relatively heavy Sb atoms (whose atomic number is 51) on the surface because of its low volatility [40], leading to a weakened axial growth and an enhanced lateral growth, since the lateral growth takes place during the VLS-dominated growth of GaAs NWs, as shown in Figure 2a. While VLS-axial growth terminates, direct MBE deposition of GaSb continues, dramatically changing the sidewall morphology and resulting in very rough facets along the growth direction of NWs and undulating sidewalls, as shown in Figure 1d. Moreover, the growth temperature we adopted was 380 °C, which is lower enough than that of previous reports [30,41]. The diffusion ability of adatoms lessens as temperature drops, making a lower temperature favorable for VS-dominated lateral growth. Thus, sidewall nucleation and growth of GaSb shells start on the grown GaAs NWs with the introduction of Sb, under the joint influence of these factors, leading to the formation of GaAs/GaSb core-shell heterostructured NWs.

Additionally, owing to the absence of Au droplets, GaSb deposited on the top region of NWs undergoes VS mechanism, similar to the growth of GaSb shells. The morphology was restrained by Wulff construction [42,43], in which facets with low surface energies are preserved, while facets with high surface energies disappear, giving rise to the formation of bulgy GaSb particles on NW tips [44].

As for the GaSb shell with a wurzite-dominant structure, this finding has seldom been discussed before. It has been reported that shell layers would take the same structure as their core NWs during the growth of core-shell NWs, such as InAs/InP [45], GaAs/InAs [31,46], and GaAs/GaAsSb [47]. The structure of shell layers, whether of wurzite or zinc-blende structure, is determined by the maximum change of Gibbs free-energy for wurzite and zinc-blende structures. Based on the VS-dominant growth mode, the Gibbs free-energy change can be described as follows [48]:

$$\Delta G_{VS} = -\frac{A\Delta\mu}{\alpha} + (P\mathrm{h} + A)\gamma_{vn} + A\gamma_{sn} \quad (1)$$

where A represents the lower (or upper) surface area of the nucleus, $\Delta\mu$ is the chemical potential difference for each pair of III-V atoms between vapor-solid phases, α is the area of III-V atoms pair on the nucleation surface, P and h are perimeter and height of each nucleus, and γ_{vn} and γ_{sn} are the vapor-nucleus interface energy and solid-nucleus interface energy, respectively. Also, there is additional wurzite to zinc-blende structure transition energy ($\Delta\gamma_{\mathrm{p}}$) for a zinc-blende nucleus on wurzite structure GaAs sidewalls, compared with the formation of a wurzite structure. In the meantime, each pair of GaSb atoms needs higher energy to form a wurzite structure (ΔE ~36 meV) than that for a zinc-blende structure, according to the density functional calculations [44]. Thus, it is preferential for GaSb to form a wurzite structure instead of a zinc-blende structure if $\Delta E < \Delta\gamma_{\mathrm{p}}$, which is expected under this growth condition. As the band-gap can be tuned by crystal structure [49], this wurzite GaAs/GaSb NW is of interest to the field of band-gap engineering.

3. Materials and Methods

GaAs/GaSb NWs were grown on GaAs(111)B substrates by Riber-32 R@D MBE system with Au particles acting as catalysts. Prior to NW growth, a pretreatment procedure including degassing and deoxidation was employed to desorb surface contaminants. Then, a 200–300 nm thick GaAs buffer layer was grown on the substrate to achieve an atomically flat surface in the growth chamber. After that, the substrate was transferred into an Au evaporation chamber, which is a buffer chamber of a typical Riber MBE system, and an ultra-thin Au film was deposited on the substrate at room temperature from the Knudsen cell. After deposition, the Au-coated substrate was transferred into the growth chamber and annealed for 5 min at a temperature of 500 °C to generate Au nanoparticles.

The GaAs substrates were under As_4 ambient overpressure to avoid decomposition during the annealing process. The NWs were grown by switching on the Ga source at the growth temperature. Each source flux was controlled by beam equivalent pressure (BEP) measured with ion gauges. GaAs stem was grown first, followed by GaSb segment. All GaAs NWs were grown for 20 min with constant As_4 (4.0×10^{-6} Torr) and Ga (2.6×10^{-7} Torr) flux BEP, respectively.

Subsequently, the As_4 source was switched off and the Sb source was opened until the GaAs NWs' growth finished. GaSb growth times were set for 1 min, 5 min and 15 min, separately, under a fixed V/III flux ratio of 1.3. Then, the Sb source and the Ga source were switched off instantly and the substrate was cooled down in As_4 ambient until 300 °C at the end of the growth period. The surface morphology of the as-grown NWs was investigated by scanning electron microscopy (SEM, FEI Sirion200). The crystal structure was characterized by transmission electron microscopy (TEM, FEI Tecnai F30) with an energy-dispersive spectroscopy (EDS) for compositional determination, operated at 300 kV.

4. Conclusions

In summary, we demonstrated MBE growth of GaAs/GaSb core-shell heterostructured NWs using Au catalysts. The structural and compositional characteristics of GaAs/GaSb NWs with different growth times for the GaSb section were investigated. Growth of the GaAs stem is VLS-dominated, while the GaSb nucleated on the sidewalls of the grown GaAs core NWs with a wurzite structure under VS growth, forming GaAs/GaSb core-shell heterostructures. This wurzite structure GaAs/GaSb core-shell NWs, caused by the movement of Au particles and Sb-induced modifications in the thermodynamic and kinetic process, would provide a significant insight into the formation of core-shell heterostructured NWs using MBE.

Acknowledgments: This work was supported by the National Key R@D Program of China No. 2016YFB0402401, the National Nature Science Foundation of China (Nos. 61376015 and 11634009), and the Australian Research Council. Access to the facility used in this work was made possible through The Australian Microscopy& Microanalysis Research Facility.

Author Contributions: Dong-Dong Wei, Sui-Xing Shi, Ping-Ping Chen conceived and designed the experiments; Dong-Dong Wei, Sui-Xing Shi, Xu-Tao Zhang performed the experiments; Dong-Dong Wei, Sui-Xing Shi and Ping-Ping Chen analyzed the data; Jin Zou, Chen Zhou, Feng Tian and Jing-Tao Xie contributed to analysis tools; Dong-Dong Wei and Sui-Xing Shi wrote the paper.

Conflicts of Interest: The authors declare no conflict of interest.

References

1. Gudiksen, M.S.; Lauhon, L.J.; Wang, J.; Smith, D.C.; Lieber, C.M. Growth of nanowire superlattice structures for nanoscale photonics and electronics. *Nature* **2002**, *415*, 617–620. [CrossRef] [PubMed]
2. Xia, H.; Lu, Z.Y.; Li, T.X.; Parkinson, P.; Liao, Z.M.; Liu, F.H.; Lu, W.; Hu, W.D.; Chen, P.P.; Xu, H.Y.; et al. Distinct photocurrent response of individual GaAs nanowires induced by n-type doping. *ACS. Nano* **2012**, *6*, 6005–6013. [CrossRef] [PubMed]
3. Czaban, J.A.; Thompson, D.A.; LaPierre, R.R. GaAs Core-Shell Nanowires for Photovoltaic Applications. *Nano Lett.* **2009**, *9*, 148–154. [CrossRef] [PubMed]
4. Heiss, M.; Russo-Averchi, E.; Dalmau-Mallorqui, A.; Tutuncuoglu, G.; Matteini, F.; Ruffer, D.; Conesa-Boj, S.; Demichel, O.; Alarcon-Llado, E.; Morral, A. III-V nanowire arrays: Growth and light interaction. *Nanotechnology* **2014**, *25*, 014015. [CrossRef] [PubMed]
5. LaPierre, R.R.; Chia, A.C.E.; Gibson, S.J.; Haapamaki, C.M.; Boulanger, J.; Yee, R.; Kuyanov, P.; Zhang, J.; Tajik, N.; Jewell, N. III-V nanowire photovoltaics: Review of design for high efficiency. *Phys. Status Solidi RRL* **2013**, *7*, 815–830. [CrossRef]
6. Munshi, A.M.; Weman, H. Advances in semiconductor nanowire growth on graphene. *Phys. Status Solidi RRL* **2013**, *7*, 713–726. [CrossRef]

7. Miao, J.S.; Hu, W.D.; Guo, N.; Lu, Z.Y.; Zou, X.M.; Liao, L.; Shi, S.X.; Chen, P.P.; Fan, Z.Y.; Ho, J.C. Single InAs Nanowire Room-Temperature Near-Infrared Photodetectors. *ACS Nano* **2014**, *8*, 3628–3635. [CrossRef] [PubMed]
8. Svensson, J.; Anttu, N.; Vainorius, N.; Borg, B.M.; Wernersson, L.E. Diameter-Dependent Photocurrent in InAsSb Nanowire Infrared Photodetectors. *Nano Lett.* **2013**, *13*, 1380–1385. [CrossRef] [PubMed]
9. Kuo, C.H.; Wu, J.M.; Lin, S.J.; Chang, W.C. High sensitivity of middle-wavelength infrared photodetectors based on an individual InSb nanowire. *Nanoscale Res. Lett.* **2013**, *8*, 327. [CrossRef] [PubMed]
10. Van den Berg, J.W.G.; Nadj-Perge, S.; Pribiag, V.S.; Plissard, S.R.; Bakkers, E.P.A.M.; Frolov, S.M.; Kouwenhoven, L.P. Fast Spin-Orbit Qubit in an Indium Antimonide Nanowire. *Phys. Rev. Lett.* **2013**, *110*, 06680. [CrossRef] [PubMed]
11. Frolov, S.M.; Plissard, S.R.; Nadj-Perge, S.; Kouwenhoven, L.P.; Bakkers, E.P.A.M. Quantum computing based on semiconductor nanowires. *MRS Bull.* **2013**, *38*, 809–815. [CrossRef]
12. Ertekin, E.; Greaney, P.A.; Chrzan, D.C.; Sands, T.D. Equilibrium limits of coherency in strained nanowire heterostructures. *J. Appl. Phys.* **2005**, *97*, 114325–114334. [CrossRef]
13. Yang, Z.; Dou, X.C. Emerging and Future Possible Strategies for Enhancing 1D Inorganic Nanomaterials-based Electrical Sensors towards Explosives Vapors Detection. *Adv. Funct. Mater.* **2016**, *26*, 2406–2425. [CrossRef]
14. Dasgupta, N.P.; Yang, P.D. Semiconductor nanowires for photovoltaic and photoelectrochenmical energy conversion. *Front. Phys.* **2014**, *9*, 289–302. [CrossRef]
15. Wang, N.; Cai, Y.; Zhang, R.Q. Growth of nanowires. *Mater. Sci. Eng. R Rep.* **2008**, *60*, 1–51. [CrossRef]
16. Paladugu, M.; Zou, J.; Guo, Y.N.; Auchterlonie, G.J.; Kim, Y.; Joyce, H.J.; Gao, Q.; Tan, H.H.; Jagadish, C. Novel Growth Phenomena Observed in Axial InAs/GaAs Nanowire Heterostructures. *Small* **2007**, *3*, 1873–1877. [CrossRef] [PubMed]
17. Paladugu, M.; Zou, J.; Guo, Y.N.; Zhang, X.; Kim, Y.; Joyce, H.J.; Gao, Q.; Tan, H.H.; Jagadish, C. Nature of heterointerfaces in GaAs/InAs and InAs/GaAs axial nanowire heterostructures. *Appl. Phys. Lett.* **2008**, *93*, 101911. [CrossRef]
18. Paladugu, M.; Zou, J.; Auchterlonie, G.J.; Guo, Y.N.; Kim, Y.; Joyce, H.J.; Gao, Q.; Tan, H.H.; Jagadish, C. Evolution of InAs branches in InAs/GaAs nanowire heterostructures. *Appl. Phys. Lett.* **2007**, *91*, 133115. [CrossRef]
19. Dimakis, E.; Lahnemann, J.; Jahn, U.; Breuer, S.; Hilse, M.; Geelhaar, L.; Riechert, H. Self-Assisted Nucleation and Vapor-Solid Growth of InAs Nanowires on Bare Si(111). *Cryst. Growth. Des.* **2011**, *11*, 4001–4008. [CrossRef]
20. Lee, J.S.; Brittman, S.; Yu, D.; Park, H. Vapor-liquid-solid and vapor-solid growth of phase-change Sb2Te3 nanowires and Sb2Te3/GeTe nanowire heterostructures. *J. Am. Chem. Soc.* **2008**, *130*, 6252–6258. [CrossRef] [PubMed]
21. Jiang, X.C.; Xiong, Q.H.; Nam, S.; Qian, F.; Li, Y.; Lieber, C.M. InAs/InP radial nanowire heterostructures as high electron mobility devices. *Nano Lett.* **2007**, *7*, 3214–3218. [CrossRef] [PubMed]
22. Treu, J.; Bormann, M.; Schmeiduch, H.; Doblinger, M.; Morkotter, S.; Matich, S.; Wiecha, P.; Saller, K.; Mayer, B.; Bichler, M. Enhanced luminescence properties of InAs-InAsP core–shell nanowires. *Nano Lett.* **2013**, *13*, 6070–6077. [CrossRef] [PubMed]
23. Balgos, M.H.; Jaculbia, R.; Defensor, M.; Afalla, J.P.; Ibanes, J.J.; Bailon-Somintac, M.; Estacio, E.; Salvador, A.; Somintac, A. Shell to core carrier-transfer in MBE-grown GaAs/AlGaAs core-shell nanowires on Si(100) substrates. *J. Lumin.* **2014**, *155*, 27–31. [CrossRef]
24. Gao, Q.; Tan, H.H.; Jackson, H.E.; Smith, L.M.; Yarrison-Rice, J.M.; Zou, J.; Jagadish, C. Growth and properties of III-V compound semiconductor heterostructure nanowires. *Semicond. Sci. Technol.* **2012**, *27*, 059501. [CrossRef]
25. Zhou, H.L.; Hoang, T.B.; Dheeraj, D.L.; van Helvoort, A.T.J.; Liu, L.; Harmand, J.C.; Fimland, B.O.; Weman, H. Wurtzite GaAs/AlGaAs core-shell nanowires grown by molecular beam epitaxy. *Nanotechnology* **2009**, *20*, 415701. [CrossRef] [PubMed]
26. Skold, N.; Karlsson, L.S.; Larsson, M.W.; Pistol, M.E.; Seifert, W.; Tragardh, J.; Samuelson, L. Growth and optical properties of strained GaAs-GaxIn1-xP core-shell nanowires. *Nano Lett.* **2005**, *5*, 1943–1947. [CrossRef] [PubMed]

27. Ganjipour, B.; Sepehri, S.; Dey, A.W.; Tizno, O.; Borg, B.M.; Dick, K.A.; Samuelson, L.; Wernersson, L.E.; Thelander, C. Electrical properties of GaSb/InAsSb core/shell nanowires. *Nanotechnology* **2014**, *25*, 25201–25201. [CrossRef] [PubMed]
28. Ganjipour, B.; Ek, M.; Borg, B.M.; Dick, K.A.; Pistol, M.E.; Wernersson, L.E.; Thelander, C. Carrier control and transport modulation in GaSb/InAsSb core/shell nanowires. *Appl. Phys. Lett.* **2012**, *101*, 103501. [CrossRef]
29. Webb, J.L.; Kuntsson, J.; Hjort, M.; Ghalamestani, S.G.; Dick, K.A.; Timm, R.; Mikkelsen, A. Electrical and Surface Properties of InAs/InSb Nanowires Cleaned by Atomic Hydrogen. *Nano Lett.* **2015**, *15*, 4865–4875. [CrossRef] [PubMed]
30. Jeppsson, M.; Dick, K.A.; Wagner, J.B.; Caroff, P.; Deppert, K.; Samuelson, L.; Wernersson, L.E. GaAs/GaSb nanowire heterostructures grown by MOVPE. *J. Cryst. Growth.* **2008**, *310*, 4115–4121. [CrossRef]
31. Paladugu, M.; Zou, J.; Guo, Y.N.; Zhang, X.; Joyce, H.J.; Gao, Q.; Tan, H.H.; Jagadish, C.; Kim, Y. Evolution of Wurtzite Structured GaAs Shells Around InAs Nanowire Cores. *Nanoscale Res. Lett.* **2009**, *4*, 846–849. [CrossRef] [PubMed]
32. Zou, J.; Paladugu, M.; Wang, H.; Auchterlonie, G.J.; Guo, Y.N.; Kim, Y.; Gao, Q.; Joyce, H.J.; Tan, H.H.; Jagadish, C. Growth Mechanism of Truncated Triangular III-V Nanowires. *Small* **2007**, *3*, 389–393. [CrossRef] [PubMed]
33. Zhang, Z.; Lu, Z.Y.; Xu, H.Y.; Chen, P.P.; Lu, W.; Zou, J. Structure and quality controlled growth of InAs nanowires through catalyst engineering. *Nano Res.* **2014**, *7*, 1640–1649. [CrossRef]
34. Zhang, Z.; Shi, S.X.; Chen, P.P.; Lu, W.; Zou, J. Influence of substrate orientation on the structural quality of GaAs nanowires in molecular beam epitaxy. *Nanotechnology* **2015**, *26*, 255601. [CrossRef] [PubMed]
35. Pan, D.; Fu, M.Q.; Yu, X.Z.; Wang, X.L.; Zhu, L.J.; Nie, S.H.; Wang, S.L.; Chen, Q.; Xiong, P.; von Molnar, S. Controlled Synthesis of Phase-Pure InAs Nanowires on Si(111) by Diminishing the Diameter to 10 nm. *Nano Lett.* **2014**, *14*, 1214–1220. [CrossRef] [PubMed]
36. Wang, Y.W.; Schmidt, V.; Senz, S.; Gosele, U. Epitaxial growth of silicon nanowires using an aluminium catalyst. *Nat. Nanotechnol.* **2006**, *1*, 186–189. [CrossRef] [PubMed]
37. Hannon, J.B.; Kodambaka, S.; Ross, F.M.; Tromp, R.M. The influence of the surface migration of gold on the growth of silicon nanowires. *Nature* **2006**, *440*, 69–71. [CrossRef] [PubMed]
38. Pecora, E.F.; Irrera, A.; Priolo, F. Influence of O contamination and Au cluster properties on the structural features of Si nanowires. *Thin Solid Films* **2010**, *518*, 2562–2564. [CrossRef]
39. Dubrovskii, V.G.; Sibirev, N.V.; Cirlin, G.E.; Soshnikov, I.P.; Chen, W.H.; Larde, R.; Cadel, E.; Pareige, P.; Xu, T.; Grandidier, B. Gibbs-Thomson and diffusion- induced contributions to the growth rate of Si, InP, and GaAs nanowires. *Phys. Rev. B* **2009**, *79*, 205316. [CrossRef]
40. Dimroth, F.; Agert, C.; Agert, A.W. Growth of Sb-based materials by MOVPE. *J. Cryst. Growth* **2003**, *248*, 265–273. [CrossRef]
41. Borg, B.M.; Dick, K.A.; Ganjipour, B.; Pistol, M.E.; Wernersson, L.E.; Thelander, C. InAs/GaSb Heterostructure Nanowires for Tunnel Field-Effect Transistors. *Nano Lett.* **2010**, *10*, 4080–4085. [CrossRef] [PubMed]
42. Moll, N.; Kley, A.; Pehlke, E.; Scheffler, M. GaAs equilibrium crystal shape from first principles. *Phys. Rev. B* **1996**, *54*, 8844–8855. [CrossRef]
43. Wulff, G.Z. On the question of speed of growth and dissolution of crystal surfaces. *Z. Kristallogr.* **1901**, *34*, 449–530.
44. Shi, S.X.; Zhang, Z.; Lu, Z.Y.; Shu, H.B.; Chen, P.P.; Li, N.; Zou, J.; Lu, W. Evolution of morphology and microstructure of GaAs/GaSb nanowire heterostructures. *Nanoscale Res. Lett.* **2015**, *10*, 108. [CrossRef] [PubMed]
45. Liu, X.Y.; Liu, P.B.; Huang, H.; Chen, C.X.; Jin, T.N.; Zhang, Y.F. Growth and large-scale assembly of InAs/InP core/shell nanowire: Effect of shell thickness on electrical characteristics. *Nanotechnology* **2013**, *24*, 245306. [CrossRef] [PubMed]
46. Rieger, T.; Schapers, T.; Grutzmacher, D.; Lepsa, M.I. Crystal phase selective growth in GaAs/InAs core-shell nanowires. *Cryst. Growth Des.* **2014**, *14*, 1167–1174. [CrossRef]
47. Ghalamestani, S.G.; Munshi, A.M.; Dheeraj, D.L.; Fimland, B.O.; Weman, H.; Dick, K.A. Self-catalyzed MBE grown GaAs/$GaAs_xSb_{1-x}$ core-shell nanowires in ZB and WZ crystal structures. *Nanotechnology* **2013**, *24*, 405601. [CrossRef] [PubMed]

48. Markov, I.V. *Crystal Growth for Beginners: Fundamentals of Nucleation, Crystal Growth, and Epitaxy*, 2nd ed.; World Scientific Publishing Company: Singapore, 2006.
49. Zanolli, Z.; Fuchs, F.; Furthmueller, J.; von Barth, U.; Bechstsdt, F. Model GW band structure of InAs and GaAs in the wurzite phase. *Phys. Rev. B* **2007**, *75*, 245121. [CrossRef]